KSME

Springer

Journal of Mechanical Science and Technology 37 (5) 2023

Original Article
DOI 10.1007/s12206-023-0430-9

Keywords:
· Running-in performance
· System stability
· 2D ultrasonic burnishing
· 7075 aluminum alloy

Correspondence to:
Zhongyu Piao
piaozy@zjut.edu.cn

Citation:
Ding, C., Feng, S., Qiao, Z., Zhou, Z., Piao, Z. (2023). Running-in performance of 7075 aluminum alloy strengthened by burnishing technology. Journal of Mechanical Science and Technology 37 (5) (2023) 2545~2553.
http://doi.org/10.1007/s12206-023-0430-9

Received November 16th, 2022
Revised January 2nd, 2023
Accepted January 3rd, 2023

† Recommended by Editor
Hyung Wook Park

Running-in performance of 7075 aluminum alloy strengthened by burnishing technology

Cong Ding[1,2,3], Shiqing Feng[1,2], Zhizhao Qiao[1,2], Zhenyu Zhou[1,2] and Zhongyu Piao[1,2]

[1]College of Mechanical Engineering, Zhejiang University of Technology, Hangzhou 310023, China, [2]Key Laboratory of Special Purpose Equipment and Advanced Processing Technology, Ministry of Education and Zhejiang Province, Zhejiang University of Technology, Hangzhou 310023, China, [3]State Key Laboratory of Engine Reliability, Weifang 261001, China

Abstract A 2D ultrasonic burnishing technology was employed to strengthen 7075 aluminum alloy. The running-in experiments for original and burnished samples were implemented, and the running-in performance was explored qualitatively and quantitatively. The results show that the worn surface of an original sample exhibited the peelings, scratches, and abrasive particles, yet the wear form of a burnished sample was relatively single, mainly with scratches. The quantitative parameter "maximum distance between phase points d_{max}" was calculated. During the friction and wear process, the d_{max} of friction coefficient signal displayed the variation of first decreasing and then stabilizing, which was consistent with the running-in and steady-state stages of the friction system. Compared with the original sample, the burnished sample had a less d_{max}, which indicated that the phase trajectory had a more convergence, and the friction system had a better stability. This study can guide surface strengthening and running-in performance analysis.

1. Introduction

High-end equipment technology in deep space, deep ocean, and polar environment is the critical development direction of the Chinese manufacturing industry. In a harsh environment, 7075 aluminum alloy as a friction component inevitably incurs wear failure [1, 2]. The necessary strengthening techniques are implemented to improve the finish surface and wear property of 7075 aluminum alloy, wherein the burnishing processing operation gets a wide attention from researchers. The burnishing technology, a cold working processing, utilizes pressure to promote surface plastic deformation, so as to improve the surface roughness and hardness [3].

El-Axir et al. [4] investigated the effect of ball burnishing process on the surface finishing of 2014 aluminum alloy, and the experimental results indicated that the surface roughness decreased from 4 μm to 0.14 μm. Lv et al. [5] used burnishing technology to process 2024 aluminum alloy and obtained different burnished layers. The results showed that the burnished layers showed fine grains and the surface corrosion resistance was improved. Khalilpourazary and Salehi [6] utilized roller burnishing to process 7175 aluminum alloy and found that the burnished surface had higher microhardness. To further optimize the aluminum alloy surface, ultrasonic-assisted technology was used in burnishing. For instance, Teimouri [7] utilized ultrasonic-assisted burnishing to maximize the value of surface compressive residual stress. Liu et al. [8] employed two-dimensional (2D) ultrasonic roller burnishing to process 7050 aluminum alloy and then characterized the surface performance. The experimental results illustrated that the residual stress of the burnished surface was increased, and it ensured surface fatigue strengthening. Zhou et al. [9, 10] studied the wear property of 7075 aluminum alloy processed by 2D ultrasonic burnishing, and they found that the ultrasonic-assisted technique could improve surface roughness and hardness. Xia et al. [11] found that the wear volume of

burnished 6061 aluminum alloy was 21.5 % less than that of an unburnished sample via fretting wear experiments.

Commonly, the wear property of a burnished sample is investigated via the wear volume, wear rate, or wear scratch depth. These wear parameters are difficult to monitor online, so they cannot serve intelligent monitoring in the wear process. Moreover, wear is a nonlinear and dynamic process, the system behavior is dependent on working condition parameters [12, 13]. To reveal the real-time characteristics of a friction system, the friction coefficient signals can be employed, which can be on-line extracted from the system via a torque sensor [14]. In addition, the running-in process is a very significant stage, which directly affects the system stability. Therefore, in this study, 2D ultrasonic burnishing technique were used to process 7075 aluminum alloy. Then, the running-in experiments of original and burnished 7075 aluminum alloy samples were conducted on a ball-on-plate reciprocating tribometer. Finally, a nonlinear method was employed to analyze the running-in performance to determine the system stability.

2. Experiments

2.1 Ultrasonic burnishing experiments

A 2D ultrasonic burnishing apparatus is shown in Fig. 1. This apparatus mainly included a power device, a burnishing tool, a 2D vibration platform, two ultrasonic devices, a pedestal, and a sample. The burnishing tool with a cylindrical shape was installed in the power device by a clamp. The sample was fixed on the 2D vibration platform, and the 2D vibration platform was mounted on the pedestal. The power device transmitted the normal load onto the sample via the burnishing tool; meanwhile the power device provided rotation and reciprocation motion for the burnished tool. Two ultrasonic devices provided vibration with a frequency of 20 kHz and an amplitude of 9 μm to the platform in both vertical and horizontal directions. It should be emphasized that the end plane of the burnishing tool contained 19 AISI 52100 balls uniformly distributed along the circumference, and these balls had self-rotating motion during burnishing process. The original sample was a 7075 aluminum alloy plate with 50 mm×30 mm×10 mm, as shown in Fig. 2(a). Its surface roughness and hardness were 2.490 μm and 164 HV, respectively. During burnishing, the rotating speed of the main shaft was 5000 rpm, the feed speed was 25 mm/min, and the press amount of the burnishing tool was 0.24 mm. There were six original 7075 aluminum alloy plates to be processed with the same burnishing parameters. After burnishing, via the measurement with a roughness measuring instrument and a hardness tester, the burnished 7075 aluminum alloy plates possessed a surface roughness of 0.071 μm and hardness of 252 HV, as shown in Fig. 2(b).

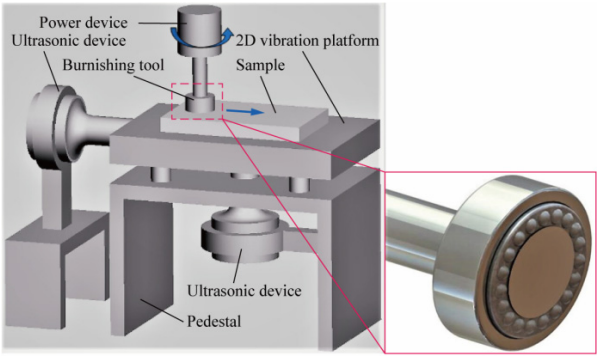

Fig. 1. Diagram of 2D ultrasonic burnishing apparatus.

Table 1. Experimental scheme.

Test	Normal load F (N)	Sample	Stroke length L (mm)	Frequency *f* (Hz)	Remarks
1	20	Original	5	2	\
2	20	Original	5	2	Repeated test
3	20	Burnished	5	2	\
4	20	Burnished	5	2	Repeated test
5	35	Original	5	2	\
6	35	Original	5	2	Repeated test
7	35	Burnished	5	2	\
8	35	Burnished	5	2	Repeated test
9	50	Original	5	2	\
10	50	Original	5	2	Repeated test
11	50	Burnished	5	2	\
12	50	Burnished	5	2	Repeated test

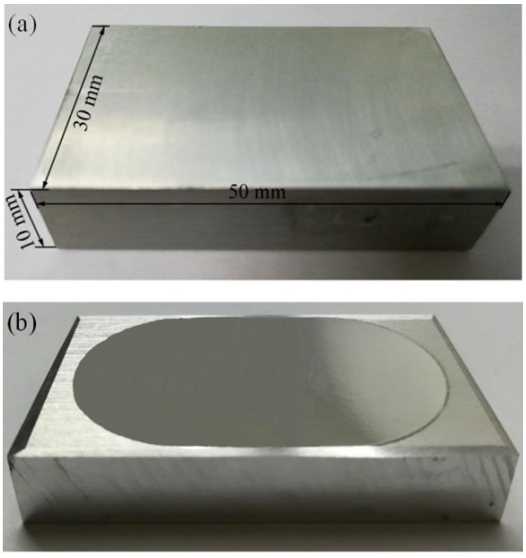

Fig. 2. Photographs of 7075 aluminum alloy samples: (a) original sample; (b) burnished sample.

2.2 Running-in experiments

Sliding running-in experiments were conducted on a reciprocating tribometer, as shown in Fig. 3. The lower sample was a burnished 7075 aluminum alloy plate. The upper sample was a ball consisting of AISI 52100 steel, and its diameter and hardness were 8 mm and 700 HV, respectively. Prior to testing, 0.05 mL lubricating oil (brand of L-HM32) was dropped onto the sample surface to be worn. The lubricating oil had a flash point of 230 °C, pour point of -15 °C, and kinematic viscosity of 33.2 cSt at 40 °C. During testing, the stroke length and the reciprocating sliding frequency were 5 mm and 2 Hz, respectively. The friction torque signal was extracted from the wear process by using a torque sensor with a sampling frequency of 300 Hz, and it was timely converted into the friction coefficient signal via a signal collecting system. The wear duration of each running-in experiment was 60 min. The detailed experimental scheme is listed in Table 1. Note each running-in experiment was repeated twice for the same working condition.

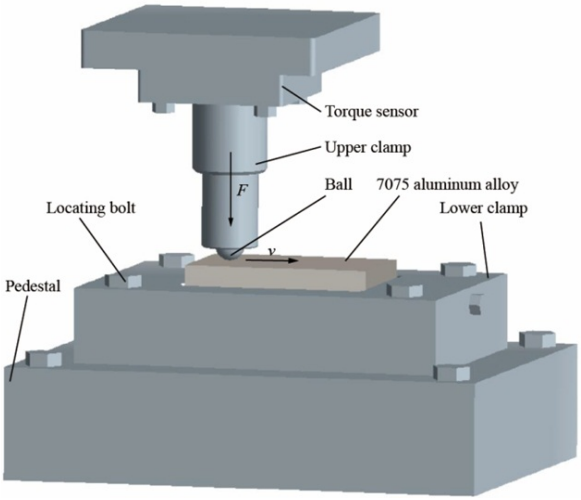

Fig. 3. Diagram of a reciprocating tribometer.

3. Experimental results

3.1 Characterization on worn surfaces

After running-in experiments, scanning electron microscope (SEM) photographs of worn surfaces of the original and burnished samples were measured and displayed in Fig. 4. Figs.

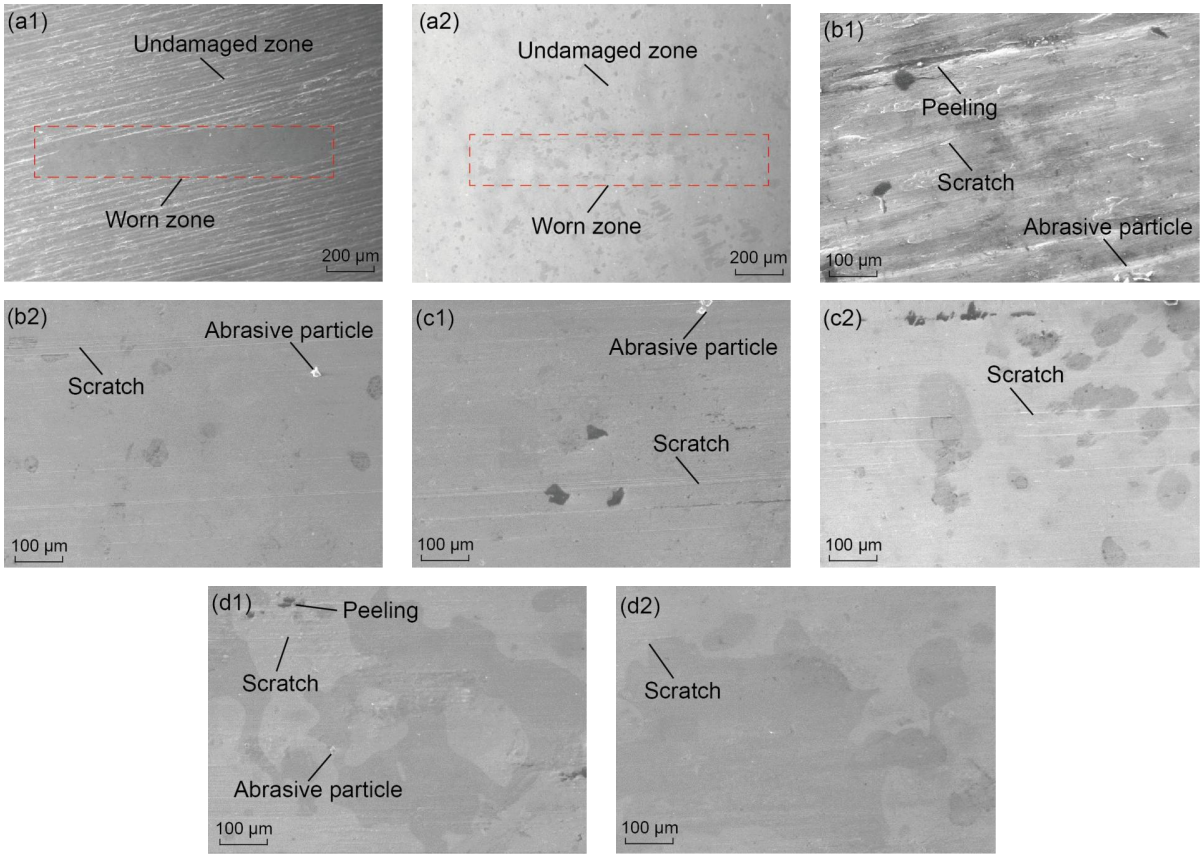

Fig. 4. SEM photographs of worn surfaces: (a1) worn zone of original sample; (a2) worn zone of burnished sample; (b1) original sample with F = 20 N; (b2) burnished samples with F = 20 N; (c1) original sample with F = 35 N; (c2) burnished samples with F = 35 N; (d1) original sample with F = 50 N; (d2) burnished samples with F = 50 N.

4(a1) and (a2) present the worn zones of original and burnished samples at 200 μm scale. For the original sample, the worn zone was obvious and relatively smooth compared with the undamaged zone with processing texture. For the burnished sample, there was a slight impression on the sample surface. Obviously, the worn zone of the burnished sample was narrower than that of the original sample. Ulteriorly, the surface topographies at 100 μm scale were characterized and displayed in Figs. 4(b1)-(d1) and (b2)-(d2). It was found that the worn zone of the original sample exhibited scratches, peelings, and abrasive particles, yet the worn zone of the burnished sample mainly exhibited some scratches.

3.2 Variation of friction coefficient signals

The time series of friction coefficient signals in all experiments are displayed in Fig. 5. As shown, the note of "F = 20 N, original-S1" represented the running-in experiment of an original sample under the normal load of 20 N, and the note of "F = 20 N, original-S2" represented the repeated experiment of the original sample under the normal load of 20 N. Likewise, the note of "F = 20 N, burnished-S1" represented the running-in experiment of a burnished sample under the normal load of 20 N, and the note of "F = 20 N, burnished-S2" represented the repeated experiment of the burnished sample under the normal load of 20 N. It was obvious that the friction coefficient signals of original or burnished samples under three kinds of normal loads had the same change trend. The specific change trend was "increasing, decreasing, and then remaining steady". This phenomenon was verified by the corresponding repeated experiments, for instance, tests 1 and 2. Generally speaking, the normal service process of metallic friction components was divided into two stages of "running-in and steady-state", and this process could be intuitively reflected via the variation of a friction coefficient signal [15]. Here, the increasing and decreasing phase of the friction coefficient signal corresponded to the running-in stage, and the steady phase of the friction coefficient signal corresponded to the steady-state stage.

4. Discussion

4.1 Qualitative analysis of running-in performances

As shown in Figs. 5(a)-(c), an initial increase in friction coefficient signal occurs because of the contact asperities of two fresh friction surfaces. The actual contact area is extremely small, so the contact pressure is enormous [16]. As the contact asperities constantly suffer wear and plastic deformation, the shape and flatness of the contact surface are gradually improved, leading to a decrease of the friction coefficient signal. Until the contact surface reaches the optimum state, the friction coefficient remains steady around the minimum. Importantly, this running-in evolution feature of the friction coefficient for 7075 aluminum alloy is consistent with the theoretical friction curve in boundary lubrication depicted in Ref. [17], as shown in Fig. 5(d).

Additionally, the maximum and mean values of the friction coefficient signals for original and burnished samples under 20, 35, and 50 N are summarized and displayed in Fig. 6. It is de-

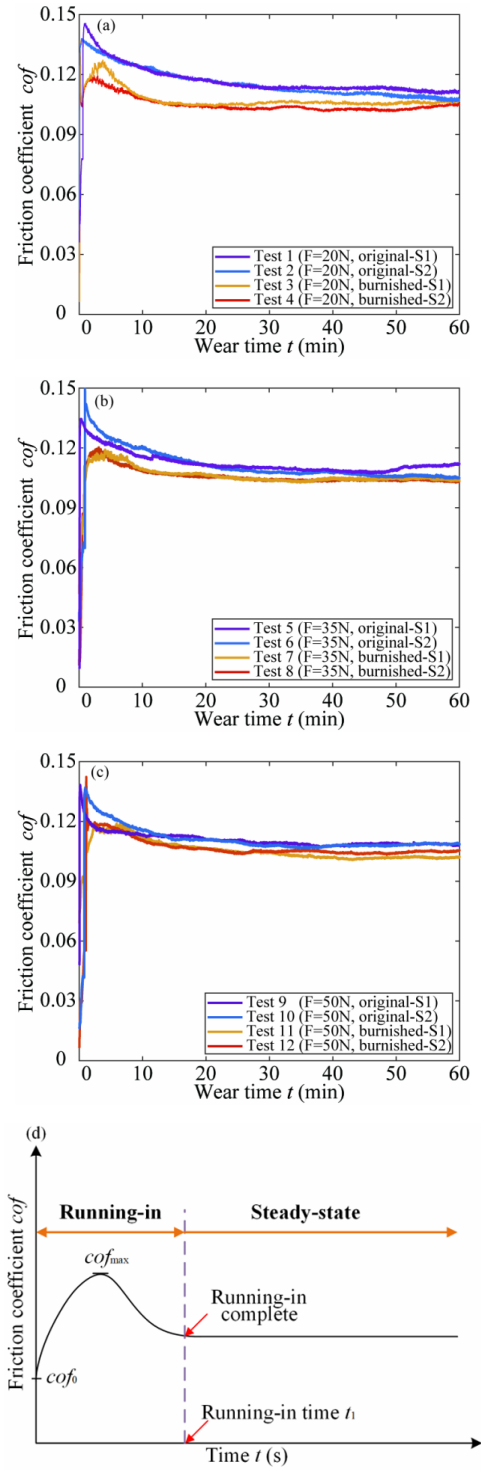

Fig. 5. Time series of friction coefficient signals: (a) F = 20 N; (b) F = 35 N; (c) F = 50 N; (d) theoretical friction curve in boundary lubrication [17].

clared that the abscissas “20 (original)” and “20 (burnished)” express the original and burnished samples under the normal load of 20 N, respectively. The legends “max(cof)-S1” and “max(cof)-S2” express the maximum friction coefficient values for the first and the repeated samples, respectively. And “mean(cof)-S1” and “max(cof)-S2” express the mean friction coefficient values for the first and the repeated samples, respectively.

As shown in Figs. 5 and 6, the friction coefficient of an original sample shows a sharp increase in the initial running-in stage. Conversely, the friction coefficient of a burnished sample shows a relatively gentle increase. And the maximum friction coefficient value of the burnished sample is clearly smaller than that of the original sample except for the repeated experiment of the burnished sample under F = 50 N. Moreover, the mean friction coefficient value of the burnished sample is smaller than that of the original sample for all the experiments. This is explained by that the burnished sample has a smaller surface roughness. The more smooth surface can effectively increase the initial contact area of friction components [16]. For the repeated experiment of the burnished sample under 50 N (test 10), a slightly larger maximum friction coefficient is mainly caused by the randomness of the contact asperities of the fresh surface. Additionally, the difference of maximum friction coefficient value between original and burnished samples is in the range of 0.0041-0.0308, and the difference of mean friction coefficient value is in the range of 0.0024-0.0126, as shown in Fig. 6. The large difference for the maximum friction coefficient can be explained as that the fresh surfaces with the same roughness have unique morphology and structure, and the initial contact asperities are significantly different. Nevertheless, the contact asperities reach the optimum in the steady-state so that the mean friction coefficient has a slight difference.

4.2 Quantitative analysis of running-in performances

The finish of running-in implies that the friction pair obtains good running-in performance. The time spent in the running-in process is termed as “running-in time” as shown in Fig. 5(d), which indicates that the friction system finishes the running-in stage and enters into the steady-state stage. Meanwhile, the friction coefficient signal experiences a gentle transition from decrease to stabilization. However, this gentle process makes it difficult to accurately determine the running-in time. As shown in Figs. 5(a)-(c), the available information is that the original and burnished samples reach the steady-state at the ranges of 20-30 min and 10-20 min, respectively. Based on researches [18], a shorter running-in time or a smaller friction coefficient value agrees with a better running-in performance, which directly affects the wear performance in steady-state. That is, the determination of running-in time plays a critical role in evaluating the running-in performance and system stability. The running-in performance refers to the friction, lubrication, deformation, and wear, and it is also affected by the working conditions, such as load, velocity and temperature [19]. It has been verified that running-in is a nonlinear process, as the system behaviors are complex and dynamic [20]. In addition, even if the friction system reaches steady-state, the internal characteristics of the system also have differences [21, 22].

Taking test 7 as an example, two segments are extracted from a stable friction coefficient signal, one is from the point 4001 to 5000, and the other is from the point 5001 to 6000. Then, the two segments containing 1000 data points are reconstructed to high-dimensional matrices, and their phase trajectories are plotted in 3D space and displayed in Fig. 7. Apparently, for the two segments consisting of adjacent steady-state data points, the starting-point positions or the

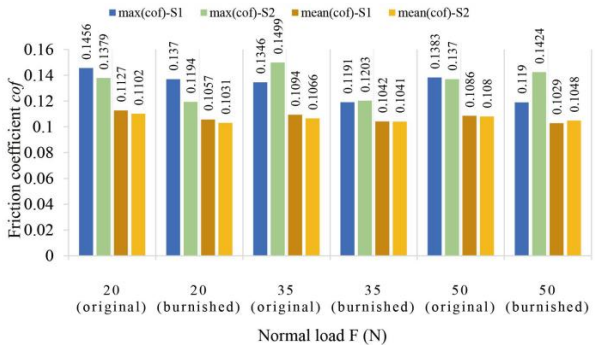

Fig. 6. Maximum and mean values of friction coefficient signals in all experiments.

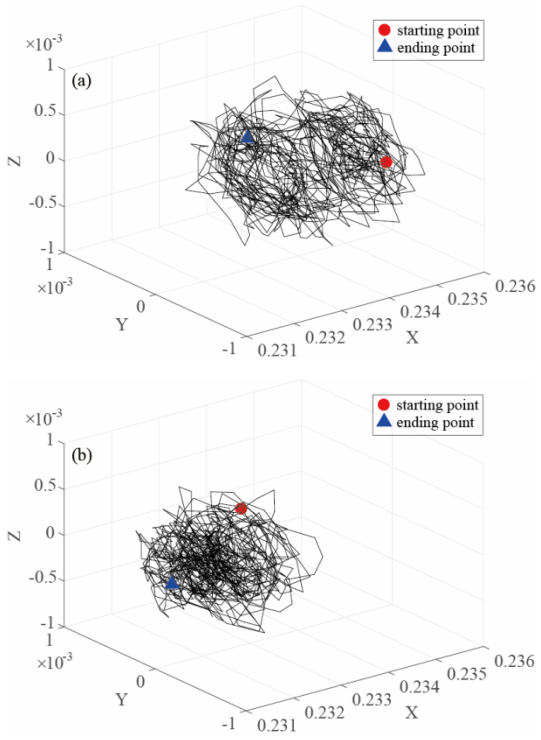

Fig. 7. Dynamic evolutions of two segments of phase trajectories in test 7: (a) data points of 4001-5000; (b) data points of 5001-6000.

ending-point positions are completely different. And the 3D shapes of the phase trajectories are also different. This performance is termed as the system inner randomness [21, 22]. That is, the frictional system in steady-state still has the internal randomness, and it is closely related to system parameters and working conditions. Namely, the univariate time series of the friction coefficient signal is difficult to exhibit the internal behavior characteristics of a friction system.

To quantify running-in performance, the univariate time series of friction coefficient signals have to be expanded to a high-dimensional space. As mentioned in Sec. 3, the repeatability of running-in experiments has been verified, so only one test is analyzed under each working condition, i.e., tests 1, 3, 5, 7, 9, 11 are analyzed in the following.

Based on Takens' theorem [23], the univariate time series $\{x_1, x_2, ..., x_n\}$ of the friction coefficient signal is reconstructed to high-dimensional matrices, given as:

$$\mathbf{X}=\begin{bmatrix}\mathbf{X}_1\\ \mathbf{X}_2\\ \vdots\\ \mathbf{X}_N\end{bmatrix}=\begin{bmatrix}x_1, & x_{1+\tau}, & x_{1+2\tau}, & \cdots, & x_{1+(m-1)\tau}\\ x_2, & x_{2+\tau}, & x_{2+2\tau}, & \cdots, & x_{2+(m-1)\tau}\\ \vdots & \vdots & \vdots & \ddots & \vdots\\ x_N, & x_{N+\tau}, & x_{N+2\tau}, & \cdots, & x_{N+(m-1)\tau}\end{bmatrix} \tag{1}$$

where, $\boldsymbol{X}_i$ is a reconstructed vector; N is the number of vector $\boldsymbol{X}_i$ in the reconstructed matrix $\boldsymbol{X}$, and $N = n-(m-1)\tau$; τ is the delaying time and calculated according to the mutual information method [24], as given in Eq. (2); m is the optimum embedding dimension and calculated by means of false nearest neighbors (FNN) [25], as given in Eq. (3).

The function of mutual information method is as

$$\mathrm{I}(S,Q)=\sum_i\sum_j P_{sq}(s_i,q_j)\log\left[\frac{P_{sq}(s_i,q_j)}{P_s(s_i)P_q(q_j)}\right] \tag{2}$$

where, S is the time series $\{x_1, x_2, ..., x_n\}$; Q is the time series $\{x_{1+\tau}, x_{2+\tau}, ..., x_{t+\tau}\}$, $(1 \le t \le n-\tau)$; namely, $\mathrm{I}(S, Q)$ is a function related with delaying time τ, $\mathrm{I}(S, Q) = \mathrm{I}(\tau)$. The first minimum value of $\mathrm{I}(\tau)$ represents that S and Q exhibit the greatest possible irrelevance, the corresponding τ is the expected delaying time.

The function of false nearest neighbors method is as

$$\left[\frac{R_{m+1}^2(i,r)-R_m^2(i,r)}{R_m^2(i,r)}\right]^{1/2}=\frac{\left|\mathbf{X}_i-\mathbf{X}_i^r\right|}{R_m(i,r)}>R_{tol} \tag{3}$$

where, R_{m+1} and R_m represent the distances between any two phase points in m+1 and m dimensional spaces, respectively; $\mathbf{X}_i$ is a phase point in m dimensional space; $\mathbf{X}_i^r$ is the nearest phase point of $\boldsymbol{X}_i$, r = 1; the threshold value R_{tol} = 15. The proportion of the false nearest neighbors decreases with the dimension m until it is less than a certain limit value or zero, at this moment, the m is the expected embedding dimension. Here, the certain limit value is set to 0.5 %. The calculation results of τ and m for tests 1, 3, 5, 7, 9, 11 are displayed in Fig. 8.

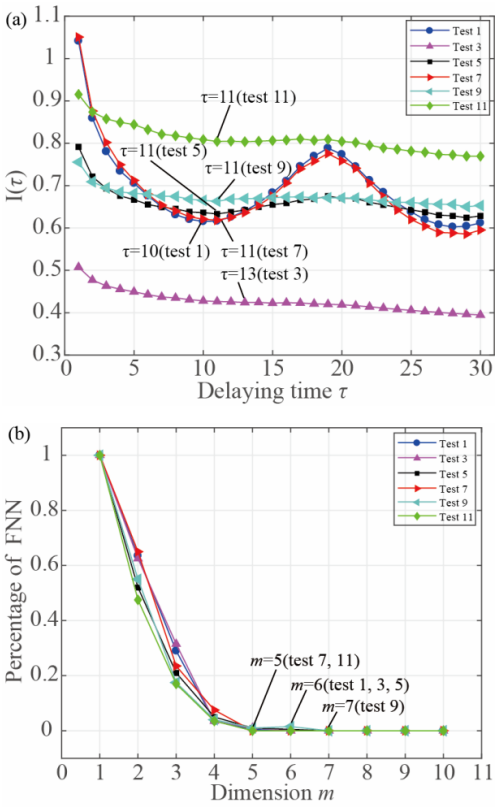

Fig. 8. Delaying times and embedding dimensions in tests 1, 3, 5, 7, 9, 11: (a) curve of I(τ)-τ; (b) curve of FNN-m.

On the basis of delaying time and embedding dimension, the univariate time series of friction coefficient signals in tests 1, 3, 5, 7, 9, 11 are reconstructed as high-dimensional matrices. For a high-dimensional matrix, each vector represents a phase point in a high-dimensional space, and the phase points constitute the phase trajectory. The size of the phase trajectory evolves with system behavior, which can be used to characterize wear states [20, 26]. The quantitative parameter "maximum distance between phase points d_{max}" is introduced to quantify the size of phase trajectory [27]:

$$d_{\max}=\max\left\{\sum_{i=1}\sum_{j=1,j\neq i}\left|\mathbf{X}_i-\mathbf{X}_j\right|\right\}. \tag{4}$$

The size of phase trajectory reflects the convergence degree of the phase trajectory. The smaller the maximum distance between phase points, the greater the convergence degree. In order to reveal the evolution feature of phase trajectory with time, for tests 1, 3, 5, 7, 9, 11, one d_{max} in each minute is calculated, so there are 60 d_{max} in total in a set of running-in experiment, as displayed in Fig. 9(a). The d_{max} in the first minute is very large, then it rapidly decreases and tends to stabilization with wear time. To better display the evolution, the d_{max} in the range of 0-0.02 is enlarged, as shown in Fig. 9(b). In the wear stage of 0-10 min, the d_{max} of the friction coefficient signal of a

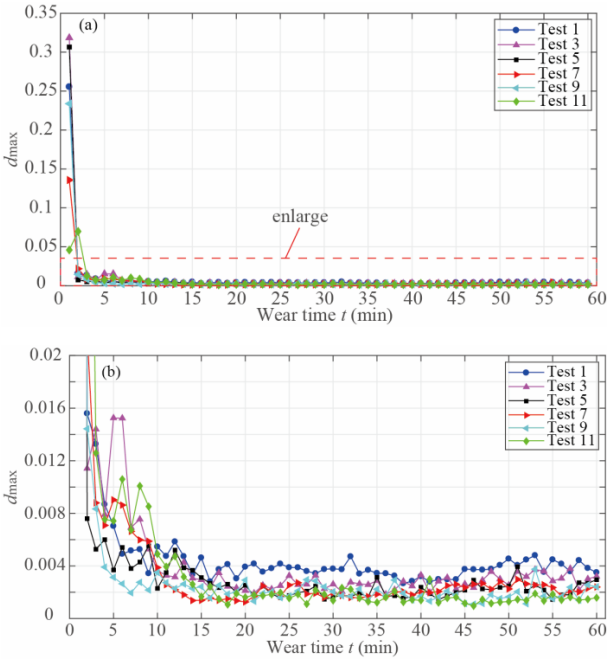

Fig. 9. Maximum distance between phase points evolving with wear time in tests 1, 3, 5, 7, 9, 11: (a) global graph; (b) partial enlarged view.

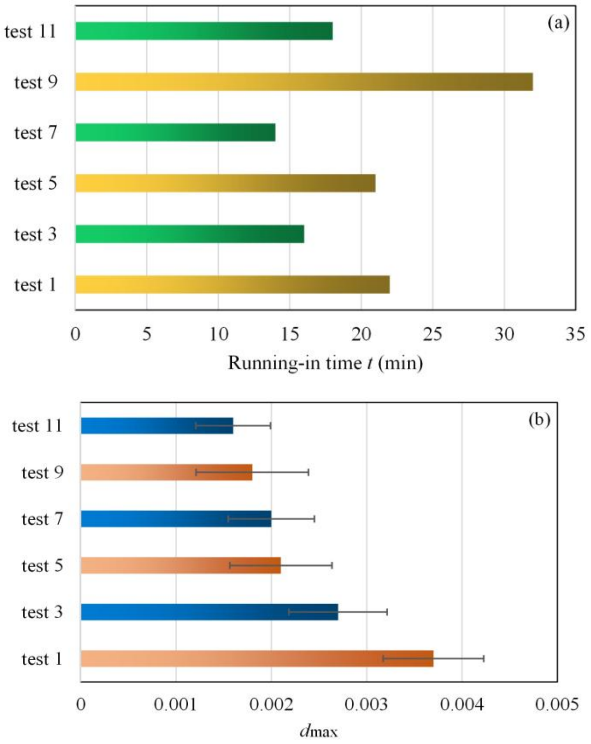

Fig. 10. Running-in time and d_{max} in test 1, 3, 5, 7, 9, 11: (a) running-in time; (b) mean value of d_{max} in steady-state.

burnished sample is larger than that of an original sample. Comparing the time series variations of friction coefficient signals in Fig. 5, the friction coefficient signal of an original sample declines steadily after experiencing a peak, yet the friction coefficient signal of a burnished sample exhibits a significant fluctuation. This explains that the d_{max} of a burnished sample is larger than that of an original sample. In the later wear stage, d_{max} is not a constant, in fact, it fluctuates in a small range, because the system behavior changes in real time even in the steady-state.

Additionally, the d_{max} keeping stable around a minimum value indicates that the running-in stage finishes, and the time spent is the running-in time. Hence, the moment when the d_{max} entering into steady-state is counted and displayed in Fig. 10(a). The running-in times of tests 1, 3, 5, 7, 9, 11 are 22 min, 16 min, 21 min, 14 min, 32 min, and 18 min in turn. Compared with the univariate time series of friction coefficient signals, the quantitative parameter d_{max} can give the accurate running-in time, which is conducive to evaluating the running-in performance. For the same friction system, a shorter running-in time indicates that the friction components reach the best matching state faster. Tests 1, 5, 9 are the wear results of original samples, and tests 3, 7, 11 are the wear results of burnished samples. It is obvious that the running-in time of the burnished sample is shorter than that of the original sample no matter what normal loads. This phenomenon illustrates that the burnishing technology is beneficial for friction components to rapidly reach the optimum contact state and enter the steady-state. Furthermore, the mean value of d_{max} in steady -state is calculated and displayed in Fig. 10(b). The mean value of d_{max} in steady-state for the burnished samples (tests 3, 7, 11) is smaller than that for the original samples (tests 1, 5, 9). A smaller d_{max} indicates that the corresponding phase trajectory has greater convergence, which means that the friction system is more stable. Thus, the system stability of a burnished sample is better than that of an original sample. In short, under the same working load, the running-in time and the system stability of the burnished sample are superior to those of the original sample.

5. Conclusions

2D ultrasonic burnishing technology was employed to strengthen the 7075 aluminum alloy surface. Then, the running-in experiments of original and burnished samples were performed under different normal loads. The worn surfaces were characterized by using SEM. Based on friction coefficient signals, the running-in performances were analyzed qualitatively and quantitatively. The main conclusions are as follows.

For the 7075 aluminum alloy, the technique of 2D ultrasonic burnishing reduces the surface roughness from micron level to nano level, from 2.490 μm to 71 nm, but also increases the hardness from 164 HV to 252 HV. For the original sample under a small normal load (F = 20 N), the worn form is mainly adhesive wear. With an increase of the normal load, the wear degree is alleviated. In comparison, the worn surface of the burnished sample is slightly worn under three normal loads. The 2D burnishing technology can significantly reduce the damage degree of the surfaces of friction components.

The running-in performance can be demonstrated by reconstructing the friction coefficient into a high-dimensional space. The decreasing maximum distance between phase points d_{max} indicates that the contact state of the friction components is adjusting to the best, and the friction system is still in running-in stage. The stabilizing d_{max} indicates that the friction system reaches the steady-state. The accurate running-in time can be obtained by the evolution of d_{max}. The burnished sample possesses a shorter running-in time, a lesser friction coefficient and less d_{max} than the original sample. It reveals that the burnished sample can acquire superior running-in performance and service lifetime.

Acknowledgments

This work is supported by the National Natural Science Foundation of China (Grant Nos. 52105215, 52175194), Zhejiang Provincial Natural Science Foundation of China (Grant No. LQ22E050016, No. LR23E050002), the Science Fund of State Key Laboratory of Engine Reliability (No. SKLER-202110), Key Laboratory of E&M (Zhejiang University of Technology), Ministry of Education & Zhejiang Province (No. EM2021120103).

References

[1] Z. Y. Li, H. Y. Yu and D. B. Sun, The tribocorrosion mechanism of aluminum alloy 7075-T6 in the deep ocean, *Corrosion Science*, 183 (2021) 109306.

[2] P. Vasanthakumar, K. Sekar and K. Venkatesh, Recent development in powder metallurgy based aluminium alloy composite for aerospace applications, *Materials Today Proceedings*, 18 (2019) 5400-5409.

[3] C. Priyadarsini, V. S. N. Ramana, K. A. Prabha and S. Swetha, A review on ball, roller, low plasticity burnishing process, *Materials Today Proceedings*, 18 (2019) 5087-5099.

[4] M. H. El-Axir, O. M. Othman and A. M. Abodiena, Study on the inner surface finishing of aluminum alloy 2014 by ball burnishing process, *J. of Materials Processing Technology*, 202 (1-3) (2008) 435-442.

[5] J. L. Lv, H. Y. Luo and T. X. Liang, Investigation of microstructure and corrosion behavior of burnished aluminum alloy by TEM, EWF, XPS and EIS techniques, *Materials Research Bulletin*, 83 (2016) 148-154.

[6] S. Khalilpourazary and J. Salehi, How alumina nanoparticles impact surface characteristics of Al7175 in roller burnishing process, *J. of Manufacturing Processes*, 39 (2019) 1-11.

[7] R. Teimouri, Optimization of residual stress field in ultrasonic assisted burnishing process, *International J. of Lightweight Materials and Manufacture*, 2 (4) (2019) 346-354.

[8] H. W. Liu, J. X. Zheng, Y. L. Guo and L. X. Zhu, Residual stresses in high-speed two-dimensional ultrasonic rolling 7050 aluminum alloy with thermal-mechanical coupling, *International J. of Mechanical Sciences*, 186 (2020) 105824.

[9] Z. Y. Zhou, Q. Y. Zheng, C. Ding, J. Y. Yan, G. J. Peng and Z. Y. Piao, Research on the promotion mechanism of surface burnishing process by two-dimensional ultrasonic vibration, *J. of Materials Research and& Technology*, 13 (2021) 1068-1082.

[10] Z. Y. Zhou, G. L. Yu, Q. Y. Zheng, G. Z. Ma, S. B. Ye, C. Ding and Z. Y. Piao, Wear behavior of 7075-aluminum after ultrasonic-assisted surface burnishing, *J. Manufacturing Processes*, 51 (2020) 1-9.

[11] W. Xia, F. L. Li, Z. Q. Tang, Z. Y. Zhou and Q. Zhao, Influence of burnishing on fretting wear behaviors of aluminum alloy 6061, *J. of South China University of Technology*, 39 (1) (2011) 84-89.

[12] M. Urbakh, J. Klafter, D. Gourdon and J. Israelachvili, The nonlinear nature of friction, *Nature*, 430 (2004) 525-528.

[13] D. Schuldberg and S. Guisinger, Nonlinear dynamical systems, chaos theory, and creativity, *Encyclopedia of Creativity*, Third Edition, Academic Press (2020) 245-254.

[14] Y. K. Zhou, H. Zhu, X. Zuo, L. Yan and N. X. Chen, The nonlinear nature of friction coefficient in lubricated sliding friction, *Tribology International*, 88 (2015) 8-16.

[15] S. Ghatrehsamani, S. Akbarzadeh and M. M. Khonsari, Experimental and numerical study of the running-in wear coefficient during dry sliding contact, *Surface Topography Metrology and Properties*, 9 (1) (2020) 015009.

[16] S. Z. Wen, P. Huang, Y. Tian and L. R. Ma, *Principles of Tribology*, Fifth Edition, Tsinghua University Press, Beijing, China (2018).

[17] P. J. Blau, *Friction and Wear Transitions of Materials*, Noyes Publications, New Jersey, USA (1989).

[18] M. M. Khonsari, S. Ghatrehsamani and S. Akbarzadeh, On the running-in nature of metallic tribo-components: a review, *Wear*, 474-475 (2021) 203871.

[19] P. J. Blau, On the nature of running-in, *Tribology International*, 38 (2005) 1007-1012.

[20] Y. K. Zhou, X. Zuo, H. Zhu and W. Tang, Development of prediction models of running-in attractor, *Tribology International,* 117 (2018) 98-106.

[21] H. Zhu, S. R. Ge, X. C. Cao and W. Tang, The changes of fractal dimensions of frictional signals in the running-in wear process, *Wear*, 263 (2007) 1502-1507.

[22] C. Ding, Property and evolution of the running-in attractor in an actual dynamic system, *Nonlinear Dynanmics*, 102 (2020) 1019-1031.

[23] F. Takens, Detecting strange attractors in turbulence, *Dynamical Systems and Turbulence*, Springer (1980) 366-381.

[24] M. T. Rosenstein, J. J. Collins and C. J. Deluca, Reconstruction expansion as a geometry-based framework for choosing proper delay times, *Physica D: Nonlinear Phenomena*, 73 (1-2) (1994) 82-98.

[25] M. B. Kennel, R. Brown and H. D. I. Abarbanel, Determining embedding dimension for phase space reconstruction using a geometrical reconstruction, *Physical Review A*, 45 (6) (1992) 3403-3411.

[26] Y. K. Zhou, X. Zuo and H. Zhu, Application of chaos theory to optimize the running-in parameters by using a running-in attractor, *Wear*, 420 (2019) 1-8.

[27] C. Ding, H. Zhu, G. D. Sun, Y. Jiang and C. L. Wei, Charac-

teristic parameter and evolution of the running-in attractor, *International J. of Bifurcation and Chaos*, 29 (4) (2019) 1950044.

Cong Ding received her Ph.D. in Mechanical Engineering from China University of Mining and Technology. She is a lecturer at the College of Mechanical Engineering, Zhejiang University of Technology, Hangzhou, China. Her current research interests include surface strengthening, tribology, signal processing, and fault monitoring.

Zhongyu Piao received his Ph.D. in Mechanical Design and Theory from Yanshan University, Qinhuangdao. He is a Professor of Mechanical Engineering, Zhejiang University of Technology, Hangzhou, China. His current research interests include tribology, surface engineering, state perception and intelligent manufacturing technology.